

# Voltage to Calcium Transformation Improves Direction Selectivity in *Drosophila* T4 neurons

Firstname Middlename Surname<sup>1\*</sup>, Firstname Middlename Familyname<sup>1,2†§</sup>,  
Firstname Initials Surname<sup>2†¶</sup>, Firstname Surname<sup>2\*</sup>

\*For correspondence:

[email1@example.com](mailto:email1@example.com) (FMS);

[email2@example.com](mailto:email2@example.com) (FS)

<sup>1</sup>Max Planck Institute of Neurobiology, Martinsried, Germany

<sup>†</sup>These authors contributed equally to this work

<sup>‡</sup>These authors also contributed equally to this work

**Present address:** <sup>§</sup>Department, Institute, Country; <sup>¶</sup>Department, Institute, Country

**Abstract** Analyzing how information is transmitted through neurons and synapses is crucial to understand how neural computation is carried out. A critical step in neural information processing is the transformation of membrane voltage into calcium signals leading to transmitter release. However, the effect of voltage to calcium transformation on neural responses to different sensory stimuli is not well understood. Here, we use in vivo, two-photon imaging of genetically encoded voltage and calcium indicators - ArcLight and GCaMP6f respectively, to measure responses in *Drosophila* direction-selective T4 neurons. Comparison between ArcLight and GCaMP6f signals revealed calcium signals to have a much higher direction selectivity compared to voltage signals. Using these recordings we further build a model which transforms T4 voltage responses to calcium responses. The model reproduces calcium responses across different visual stimuli. These findings reveal that voltage to calcium transformation involving non-linearity and low-pass filtering results in a higher direction selectivity in T4 cells.

## Introduction

In order to guide animal behavior, neurons perform a wide range of computations. Neurons encode information via dynamic changes in neuronal membrane potential. Neurons communicate mostly via chemical synapses which requires the release of neurotransmitters. When the presynaptic membrane is sufficiently depolarized, voltage-gated calcium channels open and allow  $Ca^{2+}$  to enter the cell (Luo 2020). Calcium entry leads to the fusion of synaptic vesicles with the membrane and release of neurotransmitter molecules into the synaptic cleft (Chapman 2002). As neurotransmitters diffuse across the synaptic cleft, they bind to receptors in the postsynaptic membrane, causing postsynaptic neuron to depolarize or hyperpolarize, passing the information from pre to postsynaptic neurons (Di Maio 2008). Voltage to calcium transformation in neurons is therefore a crucial step in neural information processing and neural computation.

A classic example of neural computation is how *Drosophila* neurons compute the direction of visual motion (Borst *et al.* 2020). In *Drosophila*, visual information is processed in parallel ON (contrast increments) and OFF (contrast decrements) pathways (Joesch *et al.* 2010; Eichner *et al.* 2011). Direction selectivity emerges three synapses downstream of photoreceptors, in T4 and T5 for ON and OFF pathways respectively. Four subtypes of T4 and T5 cells exist, each responding selectively to one of the four cardinal directions (Maisak *et al.* 2013). Amazingly, right at the first stage where direction selectivity emerges, T4 and T5 cells exhibit a high degree of direction selectivity, with no responses to null direction stimuli. This statement is, however, based on Calcium recordings. Whole-cell patch clamp recordings show a somewhat different picture: While preferred direction

stimuli also lead to large membrane depolarizations of -70 to -50 mV, edges or gratings moving along the null directions elicit smaller but significant responses as well (Groschner *et al.* 2022). This hints to an additional processing step where voltage signals are transformed into calcium signals that increases direction selectivity of the cells. In order to study this step systematically, we recorded both voltage and calcium signals in response to a large stimulus set that includes gratings and edges moving along various directions at different speeds and contrasts. Using these data, we build a model that captures the transformation from voltage to calcium by a few linear and non-linear processing steps.

## Results

We first expressed genetically encoded calcium indicator GCaMP6f (Chen *et al.* 2013) in T4 cells projecting to layer3 of lobula plate, and hence having upward motion as their Preferred Direction (PD) and downward motion as their Null Direction (ND). Next, we expressed genetically encoded voltage indicator Arclight (Jin *et al.* 2012) using the same driver line. Arclight's fluorescence decreases with membrane depolarization and increases with membrane hyperpolarization. To compare the voltage and calcium signals, we recorded the neural activity in T4c cells dendrites in medulla layer 10 in response to the same set of stimuli using 2-photon microscopy (Denk *et al.* 1990). The complete stimuli set included : (i) square-wave gratings of width  $30^\circ$  moving in 12 different directions, (ii) ON edge moving in PD and ND, at four different speeds ( $15^\circ$ ,  $30^\circ$ ,  $60^\circ$ ,  $90^\circ s^{-1}$ ) and four different contrasts (10%, 20%, 50%, 100%).

In a first set of experiments, we measured the voltage and calcium signals in response to gratings moving in PD and ND at four different speeds (figure 1A). As the grating stimuli consists of alternate bright and dark bars moving in a certain direction, there is a modulation in the Arclight (black traces) and GCaMP (red traces) responses to it. The GCaMP responses had modulation only for slower speeds, while Arclight responses had modulation even for faster speeds. The magnitude of response was much higher for GCaMP ( $\approx 2.0\Delta F/F$ ) compared to Arclight ( $\approx -0.06\Delta F/F$ ). The peak responses (maximum  $\Delta F/F$ ) decreased with increase in stimuli speed both for GCaMP and Arclight (figure 1B). To understand if voltage to calcium transformation affects direction selectivity in T4 cells, we compared its responses to gratings moving in PD and ND. GCaMP responses in ND were negligible compared to its responses in PD, while for Arclight responses in ND were quite visible compared to its responses in PD. We quantified the direction selectivity using a Direction Selectivity Index (DSI) calculated as the difference of the peak responses to preferred and null direction, divided by the sum of the peak responses. The results reveal a high degree of direction selectivity of close to 1 for GCaMP for slower velocities, compared to a direction selectivity of  $\approx 0.4$  for Arclight (figure 1E). For both GCaMP and Arclight signals, DSI decreased slightly with increase in velocity.

Next, instead of gratings we used a moving bright edge with all other stimulus parameters remaining the same (figure 1C). As the edge moves from bottom to top of the stimulus arena, it hits the receptive field of T4c neurons ( $\approx 15^\circ$ ) only once and there is only a single peak in the response, not a modulation as there was with gratings. The peak response decreased with increase in stimuli speed for GCaMP, while the peak response remained almost constant for Arclight throughout all speeds (figure 1D). Similar to grating responses when comparing edge responses in PD & ND, GCaMP had negligible response in ND while Arclight had considerable responses in ND compared to PD. The direction selectivity index was again much higher for GCaMP compared to Arclight (figure 1F). These results together show GCaMP signals to have high level of direction selectivity compared to Arclight signals both for grating and edge stimuli.

The stimulus strength was further varied by changing the contrast between bright and dark bars for gratings and between moving edge and background for edge stimuli. We measured Arclight and GCaMP responses to gratings moving at  $30^\circ s^{-1}$  at four different contrasts (figure 2A). Increasing contrast increases stimulus strength, resulting in an increase in response for both Arclight and GCaMP. As discussed earlier, there is a modulation in the T4c response to gratings caused

by alternate bright and dark bars. GCaMP responses however is not only modulated, but also rises steadily over time. This is interesting particularly because there is no such rise for Arclight responses. For Arclight responses we have only the modulation, whereas for GCaMP responses we have both the modulation and slow rise over time. We also measure Arclight and GCaMP responses to ON edge moving at the same speed and contrasts (figure 2C). The peak response (maximum  $\Delta F/F$ ) increased with increase in contrast (figure 2D). Similar to previous experiments, the direction selectivity index was much higher for GCaMP ( $\approx 1.0$ ) compared to that for Arclight ( $\approx 0.4$ ) (figure 2E,F).

In the results presented so far we compared responses for two directions - PD and ND. We next asked how does the comparison look if instead of two directions, responses for 12 directions are taken into account. In figure 3A, B we plot T4c Arclight & GCaMP normalized peak responses for gratings moving in 12 directions at 4 different speeds and contrasts respectively. The directional tuning is much sharper for GCaMP compared to Arclight. To quantify this we calculated the directional tuning index  $L_{dir}$  (Mazurek *et al.* 2014) for each speed and contrast stimuli condition. We calculate the index as a vector sum of the peak responses and divide the magnitude of the resultant vector by the sum of individual vector magnitudes. The directional tuning index for slower speeds and all contrasts was much higher for GCaMP ( $\approx 0.7$ ) compared to that of Arclight ( $\approx 0.2$ ). These results together show GCaMP to have a higher degree of directional tuning across different speeds and contrasts compared to Arclight.

How does the voltage to calcium transformation lead to calcium signals with significantly higher direction selectivity and tuning compared to voltage signals? To address this question, we constructed an algorithmic model (figure 4) which takes Arclight signals as inputs and outputs GCaMP signal. In order to find the optimal parameter values, we first define an error function. For each time point and stimulus condition, the error is calculated as :  $error = \sum_{i=0}^N (Model - data)^2$ . The model takes as input Arclight data across all stimuli conditions - gratings speed(48), gratings contrast(48), edge speed(8), edge contrast(8) i.e. a total of 112 different stimuli conditions. Next, the model produces output and sums the error for all stimuli conditions :  $Total\ error = \sum_{i=1}^{112} error_i$ . We then find the optimal parameters values of the model that correspond to the minimum total error using Python SciPy optimize minimize function (Virtanen *et al.* 2020).

We started with a simple model (figure 4A). The model first passes the Arclight signal through a high-pass filter. The high-pass filter brings input Arclight signal closer to actual voltage signal by removing Arclight indicator dynamics. This is followed by a threshold since voltage changes below a certain threshold does not affect the calcium level in the cell. Now, few experimental observations which we took into consideration for building up the model further were as follows : First, the GCaMP response to grating had modulation only for slower speeds, whereas Arclight showed modulations even at faster speeds (figure 1A). This suggests that the GCaMP signal is a low-pass filtered version of the Arclight signal. In the simple model, we used a single low-pass filter followed by a gain and time-shift. Multiplication with a gain factor is required since GCaMP signals have a much higher magnitude compared to Arclight. The time-shift aligns the model signal. Arclight and GCaMP responses have been recorded from different flies, therefore the responses can have different phases and a time-shift is necessary to align the signals. However, the simple model with single low-pass filter could not reproduce responses across all stimuli. The total error for complete dataset fit for the simple model was around 34%. Specifically, the simple model fails to reproduce the edge responses. Second, the GCaMP responses in addition to modulation also had a steady rise over time whereas Arclight signal only had modulation (figure 1A, 2A). For producing the edge responses and modulation in gratings responses, the model needs a low-pass filter with a smaller time constant. However to simulate the steady rise in the gratings signal the model needs a low-pass filter with a larger time constant. Hence, we combined the output of two low-pass filters. Combining the low-pass filters output with an addition (figure 4B) did not lead to much improvement with error being around 33.7% for complete dataset fit. However, combining both the outputs with a multiplication led to significant decrease in the error. The error for the multiplicative

142 model (figure 4C) was around 20%.

143 The multiplicative model thus has in total 6 parameters - high-pass filter time constant, threshold,  
144 low-pass filter 1 time constant, low-pass filter 2 time constant, gain and shift. The multiplicative  
145 model was able to reproduce calcium signals across different visual stimuli (figure 5). The model  
146 could produce both the modulation and slow rise in the GCaMP signal in response to gratings  
147 (figure 5A). The model could also reproduce the ON edge speed tuning responses across different  
148 speeds (figure 5C,D). The directional tuning index  $L_{dir}$  also were similar for model and experimental  
149 data across slower speeds and all contrasts (figure 5E,F). Thus the model is able to successfully  
150 reproduce experimental calcium data across different stimuli.

151 The slow rise in GCaMP signals over time is due to the properties of T4 cells or due to the  
152 properties of GCaMP6f. To answer this we used a faster indicator GCaMP8f (Zhang *et al.* 2020).  
153 GCaMP8f was expressed in T4c cells using the same driver line. The experiments were repeated  
154 using gratings stimuli in 12 directions at 4 speeds and ON edge in PD and ND. T4c cells GCaMP8f  
155 responses were similar to GCaMP6f responses. As with GCaMP6f, GCaMP8f signals had modulation  
156 and slow rise over time. We further compared the model parameters values for GCaMP6f data  
157 fit and GCaMP8f data fit (figure 6). The model parameters had similar values with time constants  
158 having slightly smaller values for GCaMP8f as it is a faster indicator. Therefore, the slow rise in  
159 calcium signal is indeed due to the intrinsic properties of T4 cells and not due to slowness of  
160 GCaMP6f indicator.

161 While the T4 cells' Arclight responses to gratings show only modulation, their GCaMP responses  
162 show modulation and slow increases over time. Does this response occur exclusively in direction-  
163 selective T4 cells or does it also occur in non-direction-selective cells. In order to answer this, we  
164 expressed Arclight & GCaMP6f in Mi1 & Tm3 cells, which are non-direction-selective. Mi1 & Tm3 are  
165 pre-synaptic to T4 cells and have ON-center receptive field (Arenz *et al.* 2017; Takemura *et al.* 2017).  
166 We measured Mi1, Tm3 Arclight (black) and GCaMP (red) responses to gratings moving at 4 different  
167 speeds and to gratings moving at 4 different contrasts (figure 7). The gratings were moved in only  
168 one direction, since the direction does not affect non-direction-selective cells' responses. Contrary  
169 to T4, Mi1 GCaMP responses had only modulation without a slow increase over time (figure 7A).  
170 Similar to Mi1, Tm3 GCaMP responses do not increase over time, and show only modulation for  
171 most of the stimuli conditions (figure 7A). For gratings moving at 30 deg/s and 60 deg/s, there is a  
172 slight increase in Tm3 GCaMP response over time, but the Arclight response also already has a slow  
173 increment over time. Similar to T4, the peak response for Mi1 and Tm3 decreased with an increase  
174 in speed and increased with an increase in contrast (figure 7B, D). Thus, these results together  
175 show that voltage to calcium transformation causes GCaMP response increment over time only for  
176 direction-selective T4 cells and not for non-direction-selective Mi1 and Tm3 cells.

177 Next, we used the model described in figure 4 to reproduce Mi1 and Tm3 calcium responses  
178 using their Arclight responses. As discussed earlier, the Simple model (figure 4A) with single low-  
179 pass filter was not able to reproduce T4 calcium responses across all stimuli. We had required  
180 a more complex Multiplicative model (figure 4C) using two low-pass filters for T4. However for  
181 Mi1 and Tm3, the Simple model with single low-pass filter was able to reproduce the calcium  
182 responses (figure 8). The Simple model successfully reproduces the responses for Mi1 (figure 8A)  
183 and Tm3 (figure 8C) across all stimuli conditions. The model also accurately replicates the speed  
184 and contrast tuning for Mi1 and Tm3 (figure 8B, D). We further compared the model error for  
185 Simple and Multiplicative model for Mi1, Tm3 and T4c data (figure 9). The error for Mi1 and Tm3 for  
186 Simple Model was  $\approx 6.5\%$  and  $\approx 5.9\%$  respectively compared to  $\approx 11.9\%$  and  $\approx 7\%$  respectively for  
187 the Multiplicative model. Thus the Simple model already performs better for Mi1 and Tm3 dataset  
188 and changing to Multiplicative model does not improve the performance. For T4c complete dataset  
189 the error was  $\approx 34\%$  and  $\approx 21\%$  for the Simple and Multiplicative model respectively. Hence, the  
190 Multiplicative model with two low-pass filters performs better for T4c dataset whereas for Mi1 and  
191 Tm3 the Simple model with single low-pass filter is sufficient to reproduce the calcium responses.  
192 This suggests that voltage-to-calcium transformation is more complicated for direction-selective

193 cells T4 than for non-direction-selective cells Mi1 and Tm3.

## 194 Discussion

195 Neuronal signalling and information processing involves the transformation of membrane voltage  
196 into calcium signals, which lead to transmitter release. Computations can occur in the transforma-  
197 tion between voltage and calcium or between calcium and neurotransmitter release. T4 neurons are  
198 the first direction-selective neurons found in the *Drosophila* ON motion vision pathway. Intriguingly,  
199 however, a high degree of directional selectivity is observed already at the first stage, i.e. in T4  
200 cells. In this study, we found that the voltage to calcium transformation in T4c neurons improves  
201 direction selectivity, and calcium signals in T4c cells have a much higher direction selectivity and  
202 tuning compared to membrane voltage across different stimuli conditions (figure 1-3). As calcium is  
203 required for neurotransmitter release, this would increase direction selectivity of T4c output signals.

204 Electrophysiology has been the most frequently used method to measure the membrane po-  
205 tential changes in neurons. However, due to the small size of neurons in the optic lobe, single-cell  
206 electrophysiological recordings of these neurons have been difficult. Genetically encoded voltage  
207 indicators (GEVIs) have evolved as powerful tools for recording changes in neuronal membrane  
208 potentials. Optical methods of monitoring brain activity are appealing because they allow simul-  
209 taneous, noninvasive monitoring of activity in many individual neurons. We used a fluorescence  
210 protein (FP) voltage sensor called Arclight (Jin *et al.* 2012). Arclight is based on the fusion of voltage  
211 sensing domain of *Ciona intestinalis* voltage sensitive phosphatase (Murata *et al.* 2005) and the  
212 fluorescent protein super ecliptic pHluorin with an A227D mutation. Arclight has been shown to  
213 robustly report both subthreshold events and action potentials in genetically targeted neurons in  
214 the intact *Drosophila* brain (Cao *et al.* 2013).

215 We further built a model to capture voltage to calcium transformation in T4c, Mi1 and Tm3  
216 cells. A simple model with a single low-pass filter was able to reproduce calcium responses in  
217 non-direction-selective Mi1 and Tm3 cells (figure 8), whereas a more complex model combining  
218 output of two low-pass filters via a multiplication was required to reproduce T4c calcium responses  
219 (figure 4). This suggests that voltage-calcium transformation in Mi1 and Tm3 cells is different from  
220 those in T4c cells. Differential expression of voltage-gated calcium channels in these cells could  
221 explain the different voltage to calcium transformation. Voltage-gated calcium channels mediate  
222 depolarization-induced calcium influx that drives release of neurotransmitter. The  $\alpha 1$ -subunit of  
223 the voltage-gated calcium channels forms the ion-conducting pore, which makes it distinct from  
224 other calcium channels. Three families of genes encode  $\alpha 1$  subunits. *Drosophila* genome has one  $\alpha 1$   
225 subunit gene in each family:  $\alpha 1D$  ( $Ca_v1$ ),  $cac$  ( $Ca_v2$ ), and  $\alpha 1T$  ( $Ca_v3$ ) (Littleton & Ganetzky 2000; King  
226 2007). In *Drosophila* antennal lobe projection neurons,  $cac$  ( $Ca_v2$ ) type and  $\alpha 1T$  ( $Ca_v3$ ) type voltage-  
227 gated calcium channels are involved in sustained and transient calcium currents, respectively (Gu  
228 *et al.* 2009; Iniguez *et al.* 2013). According to a RNA-sequencing study (Davis *et al.* 2020),  $\alpha 1T$  ( $Ca_v3$ )  
229 mRNA have higher expression in Mi1 (2050.16 Transcripts per Million (TPM)) compared to T4 (686.68  
230 TPM) and Tm3 (336.45 TPM). While  $cac$  ( $Ca_v2$ ) mRNA have higher expression in T4 (1298.53 TPM)  
231 compared to Mi1 (986.25 TPM) and Tm3 (817.61 TPM). Different expression of voltage-gated calcium  
232 channels could cause different voltage to calcium transformations in non-direction selective and  
233 direction-selective cells.

## 234 Materials and Methods

### 235 Flies

236 Flies (*Drosophila melanogaster*) were raised at 25°C and 60% humidity on a 12 hour light/12 hour dark  
237 cycle on standard cornmeal agar medium. For calcium imaging experiments, genetically-encoded  
238 calcium indicator GCaMP6f (Chen *et al.* 2013) was expressed in T4 neurons with axon terminals  
239 predominantly in layer 3 of the lobula plate. Similarly for voltage imaging experiments, genetically-  
240 encoded voltage indicator Arclight (Jin *et al.* 2012) was expressed in T4 layer 3 neurons. The flies

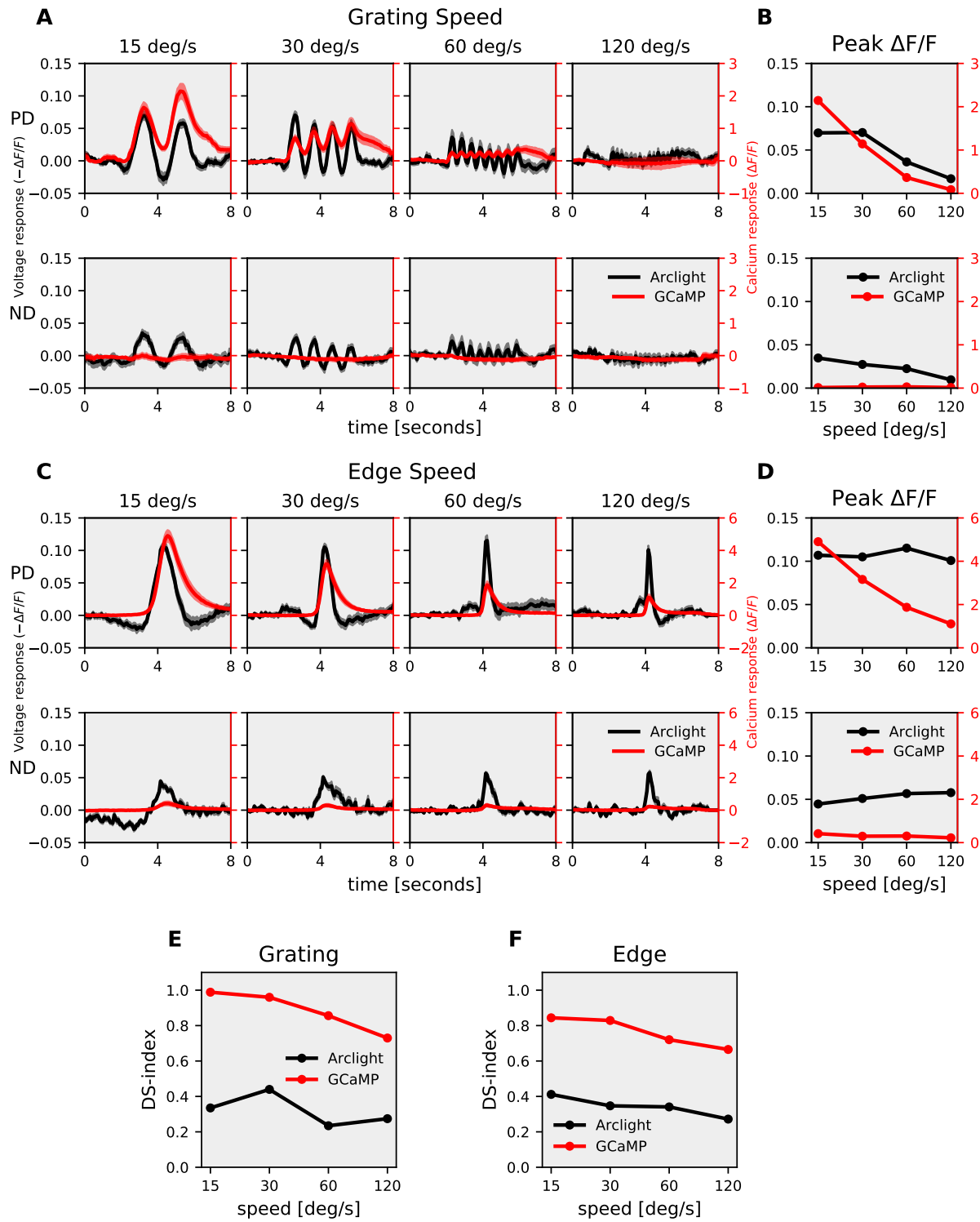


**Figure 1. T4c speed dependence :** (A) T4c Arclight (black) & GCaMP (red) responses to grating moving in PD (top row) & ND (bottom row) at 4 different speeds. Data shows the mean  $\pm$  SEM of T4c cell responses measured in 5 different flies. The plots have twin y-axis. The left y-axis of the plot represents Voltage responses i.e. changes in Arclight fluorescence ( $-\Delta F/F$ ) and the right y-axis of the plot represents Calcium responses i.e. changes in GCaMP fluorescence ( $\Delta F/F$ ) (B) T4c peak responses to grating moving in PD (top) & ND (bottom) at 4 different speeds. (C) T4c Arclight (black) & GCaMP (red) responses to ON-edge moving in PD (top row) & ND (bottom row) at 4 different speeds. Data shows the mean  $\pm$  SEM of T4c cell responses measured in 5 different flies. (D) T4c peak responses to ON-edge moving in PD & ND at 4 different speeds. (E) Direction Selectivity Index (DSI) calculated as difference of peak responses in PD and ND divided by the sum of peak responses for grating (F) Direction Selectivity Index (DSI) for ON-edge.



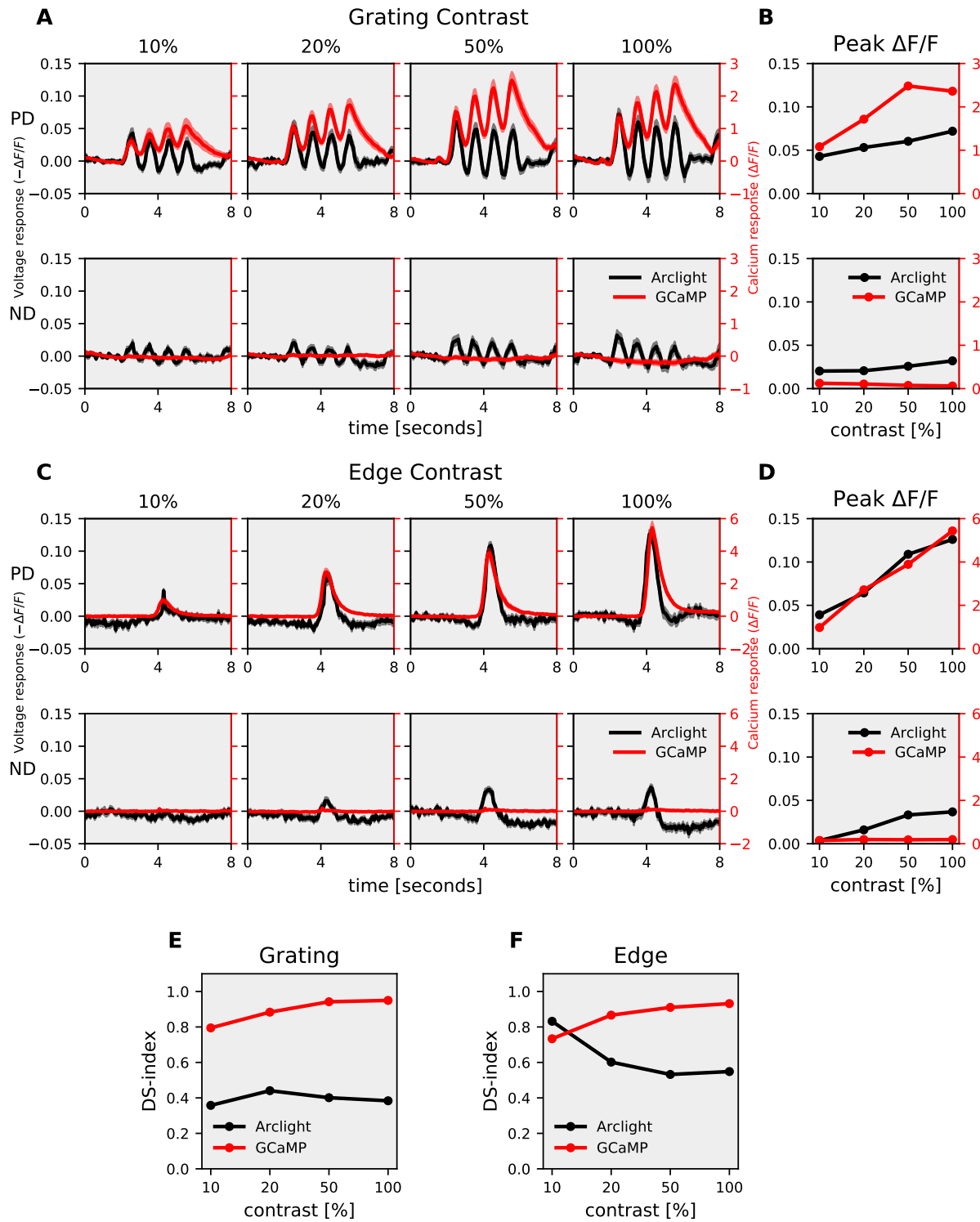


**Figure 2. T4c contrast dependence :** (A) T4c Arclight (black) & GCaMP (red) responses to grating moving in PD (top row) & ND (bottom row) at 4 contrasts. Data shows the mean  $\pm$  SEM of T4c cell responses measured in 5 different flies. The plots have twin y-axis. The left y-axis of the plot represents Voltage responses i.e. changes in Arclight fluorescence ( $-\Delta F/F$ ) and the right y-axis of the plot represents Calcium responses i.e. changes in GCaMP fluorescence ( $\Delta F/F$ ) (B) T4c peak responses to grating moving in PD (top) & ND (bottom) at 4 different contrasts. (C) T4c Arclight (black) & GCaMP (red) responses to ON-edge moving in PD (top row) & ND (bottom row) at 4 different contrasts. Data shows the mean  $\pm$  SEM of T4c cell responses measured in 5 different flies. (D) T4c peak responses to ON-edge moving in PD & ND at 4 different contrasts. (E) Direction Selectivity Index (DSI) calculated as difference of peak responses in PD and ND divided by the sum of peak responses for grating (F) Direction Selectivity Index (DSI) for ON-edge.

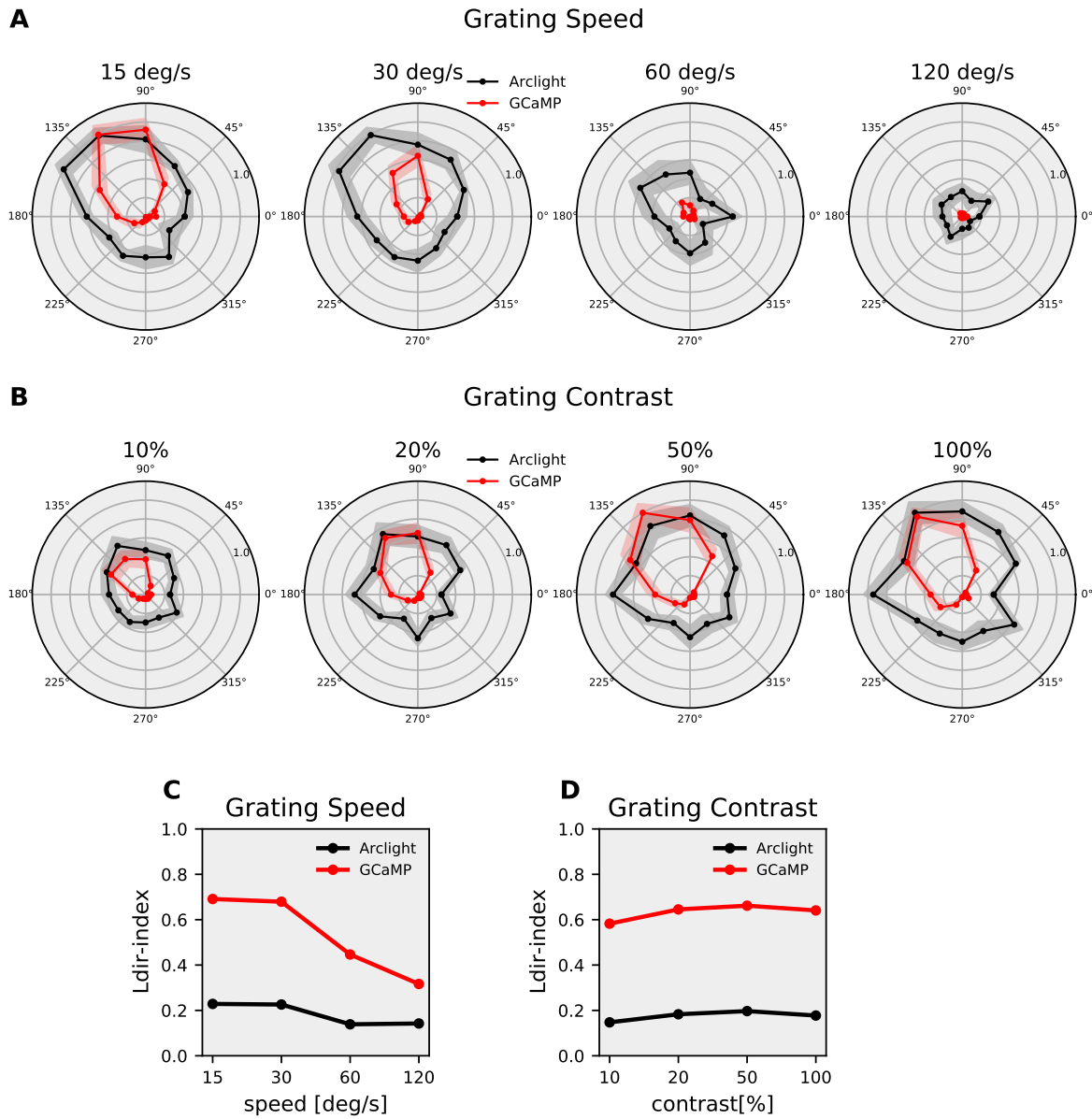


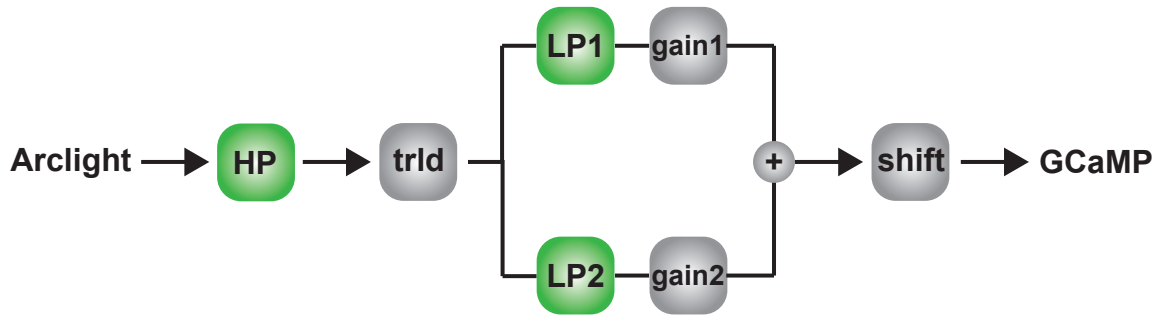
**Figure 3. T4c direction tuning** : (A) T4c Arclight (black) & GCaMP (red) normalized peak responses to grating moving in 12 directions at 4 speeds. Data shows the normalized mean  $\pm$  SEM of T4c cell peak responses measured in 5 different flies. (B) T4c Arclight (black) & GCaMP (red) normalized peak responses to grating moving in 12 directions at 4 contrasts. Data shows the normalized mean  $\pm$  SEM of T4c cell peak responses measured in 5 different flies (C) The Directional Tuning Index  $L_{dir}$  for grating moving at 4 different speeds. The Directional Tuning Index is calculated as a vector summation of the peak responses and the magnitude of resultant vector is divided by the summation of individual vector magnitudes. (D) The directional tuning index for grating at 4 different contrasts.



### A Simple Model



### B Additive Model



### C Multiplicative Model

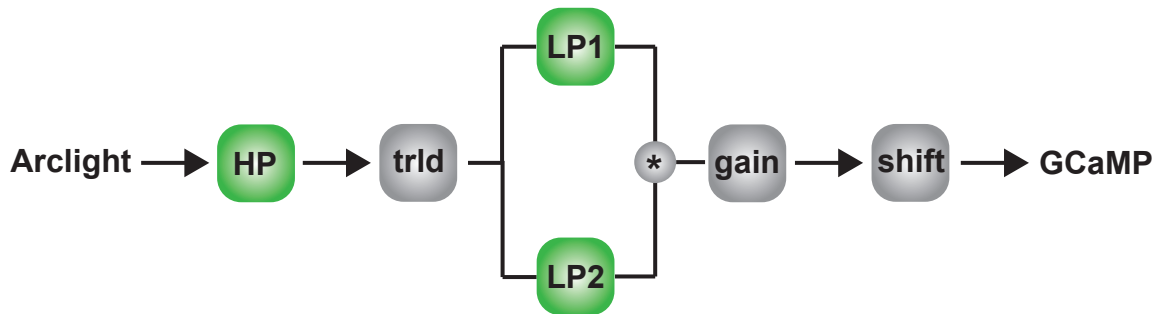


**Figure 4. Models for voltage to calcium transformation** : (A) Simple model consisting of High-Pass filter (HP), threshold(trld), Low-Pass filter(LP), gain and shift. (B) Additive model combining output of two low-pass filters via addition. (C) Multiplicative model combining output of two low-pass filters via multiplication.

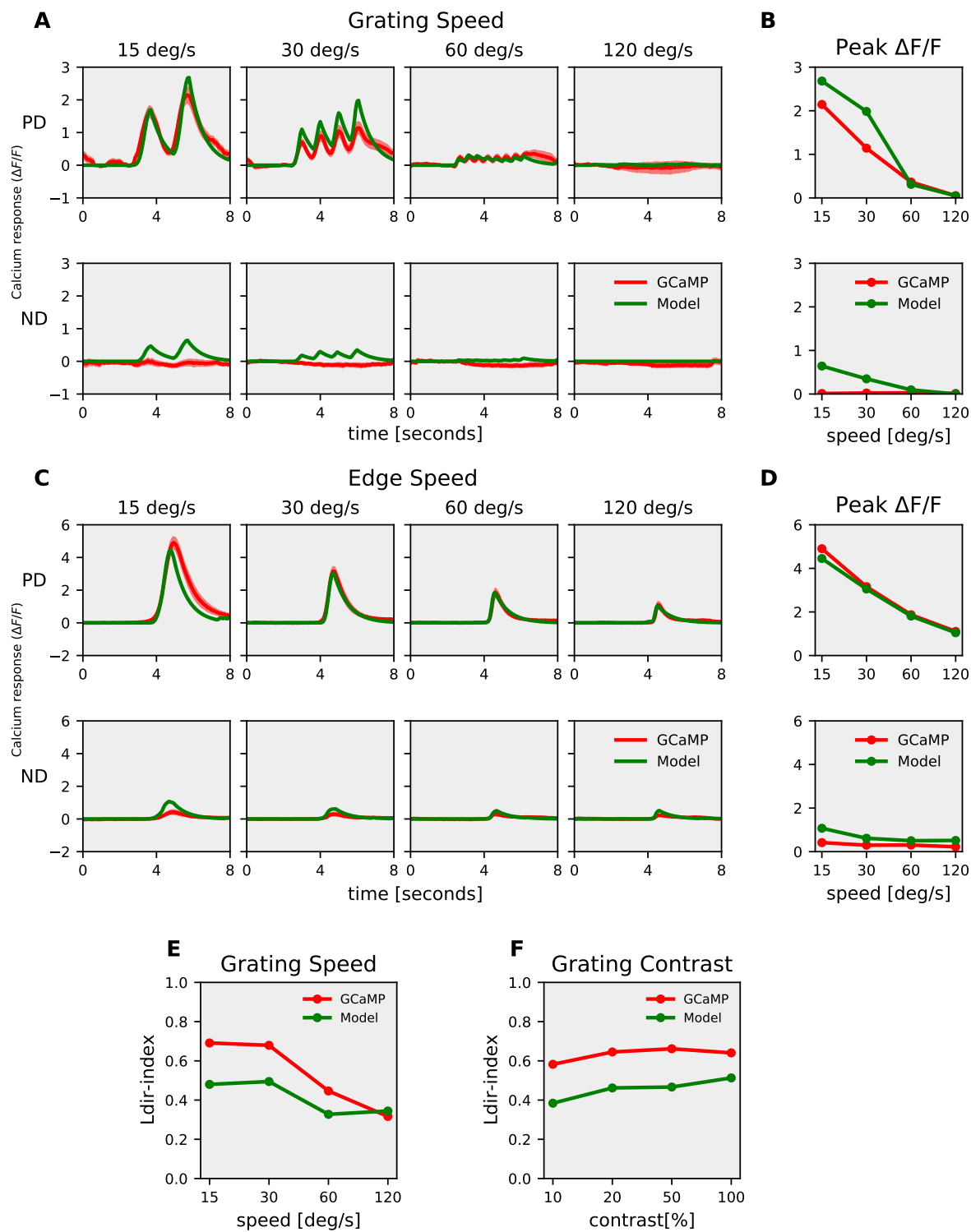


**Figure 5. Multiplicative model responses :** (A) T4c GCaMP (red) & Multiplicative model (green) responses to grating moving in PD (top row) & ND (bottom row) at 4 different speeds. (B) T4c GCaMP & model peak responses to grating moving in PD(top) & ND(bottom) at 4 different speeds. (C) T4c GCaMP (red) & Multiplicative model (green) responses to ON-edge moving in PD (top row) & ND (bottom row) at 4 different speeds. (D) T4c GCaMP & model peak responses to ON-edge moving in PD(top) & ND(bottom) at 4 different speeds. (E) The Directional Tuning Index  $L_{dir}$  for GCaMP & model for grating moving in 12 directions at 4 different speeds. (F) The Directional Tuning Index  $L_{dir}$  for GCaMP & model for grating moving in 12 directions at 4 different contrasts.

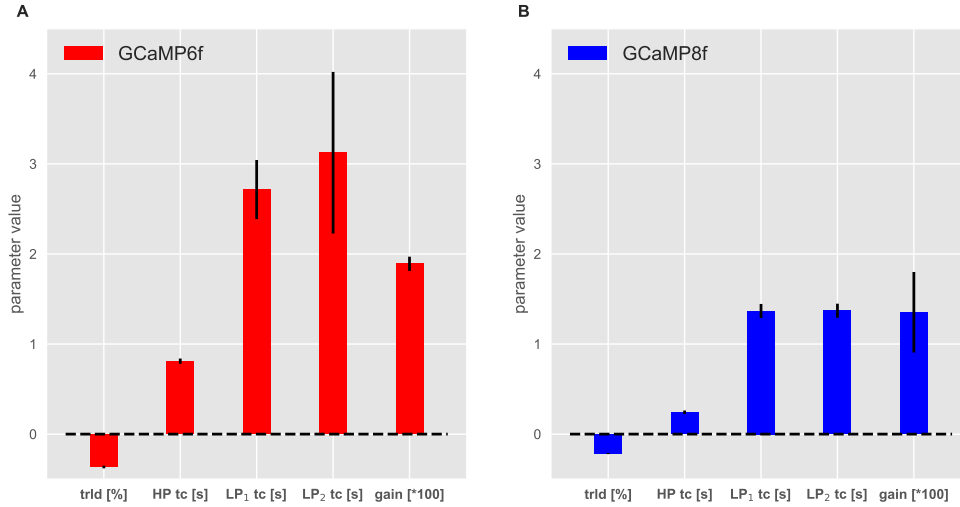


**Figure 6. Model parameters for GCaMP6f (A) and GCaMP8f (B) :** Data shows mean  $\pm$  SD for optimal parameters for the Multiplicative model. The data were fit for grating moving in 12 directions and 4 speeds, and for ON-edge moving in PD & ND at 4 speeds. trld : threshold, HP : High Pass, LP : Low Pass, tc : Time constant

genotype are as follows :

1. T4c>GCaMP6f : w+ ; VT15785-Gal4AD / UAS-GCaMP6f; VT50384-Gal4DBD / UAS-GCaMP6f
2. T4c>Arclight : w+ ; VT15785-Gal4AD / UAS-Arclight; VT50384-Gal4DBD / +

For Mi1 and Tm3 experiments, the flies genotype are as follows :

1. Mi1>GCaMP6f : w+ ; R19F01-Gal4AD / UAS-GCaMP6f; R71D01-Gal4DBD / UAS-GCaMP6f
2. Mi1>Arclight : w+ ; R19F01-Gal4AD / UAS-Arclight; R71D01-Gal4DBD / +
3. Tm3>GCaMP6f : w+ ; R13E12-Gal4AD / UAS-GCaMP6f; R59C10-Gal4DBD / UAS-GCaMP6f
4. Tm3>Arclight : w+ ; R13E12-Gal4AD / UAS-Arclight; R59C10-Gal4DBD / +

### Calcium & voltage imaging

For imaging experiments, fly surgeries were performed as previously described (Maisak *et al.* 2013). Briefly, flies were anaesthetized with CO<sub>2</sub> or on ice, fixed with their backs, legs and wings to a Plexiglas holder with back of the head exposed to a recording chamber filled with fly external solution. The cuticula at the back of the head on one side of the brain was cut away with a fine hypodermic needle and removed together with air sacks covering the underlying optic lobe. The neuronal activity was then measured from optic lobe on a custom-built 2-photon microscope as previously described (Maisak *et al.* 2013). Images were acquired at 64 x 64 pixels resolution and frame rate 13 Hz with the Scanimage software in Matlab (Pologruto *et al.* 2003).

### Visual stimulation

For the study of visual responses of T4c cells, visual stimuli were presented on a custom-built projector-based arena as described in (Arenz *et al.* 2017). In brief : Two micro-projectors (TI DLP Lightcrafter 3000) were used to project stimuli onto the back of an opaque cylindrical screen covering 180° in azimuth and 105° in elevation of the fly's visual field. To increase the refresh rate from 60 Hz to 180 Hz (at 8 bit color depth), projectors were programmed to use only green LED (OSRAM L CG H9RN) which emits light between 500 nm to 600 nm wavelength. Two long-pass filters (Thorlabs FEL0550 and FGL550) were placed in front of each projector to restrict the stimulus light to wavelengths above 550 nm. This prevents overlap between GCaMP signal and arena light spectra.

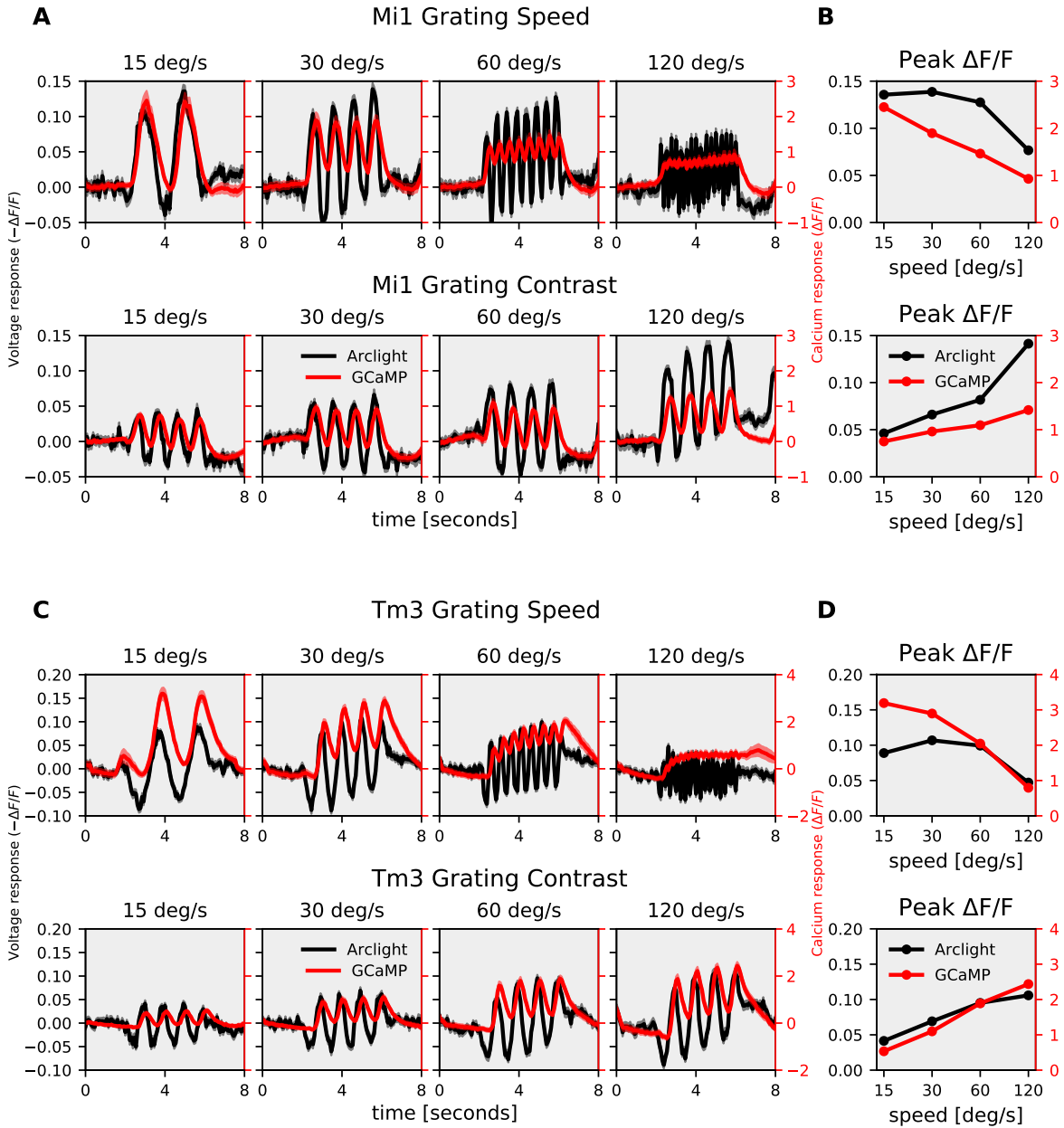


**Figure 7. Mi1, Tm3 speed and contrast dependence :** (A) Mi1 Arclight (black) & GCaMP (red) responses to grating moving at 4 different speeds. Data shows the mean  $\pm$  SEM of Mi1 cell responses measured in 5 different flies. The plots have twin y-axis. The left y-axis of the plot represents Voltage responses i.e. changes in Arclight fluorescence ( $-\Delta F/F$ ) and the right y-axis of the plot represents Calcium responses i.e. changes in GCaMP fluorescence ( $\Delta F/F$ ) (B) Mi1 peak responses to grating moving at 4 different speeds. (C) Mi1 Arclight (black) & GCaMP (red) responses to grating moving at 4 different contrasts. Data shows the mean  $\pm$  SEM of Mi1 cell responses measured in 5 different flies. (D) Mi1 peak responses to grating moving at 4 different contrasts.

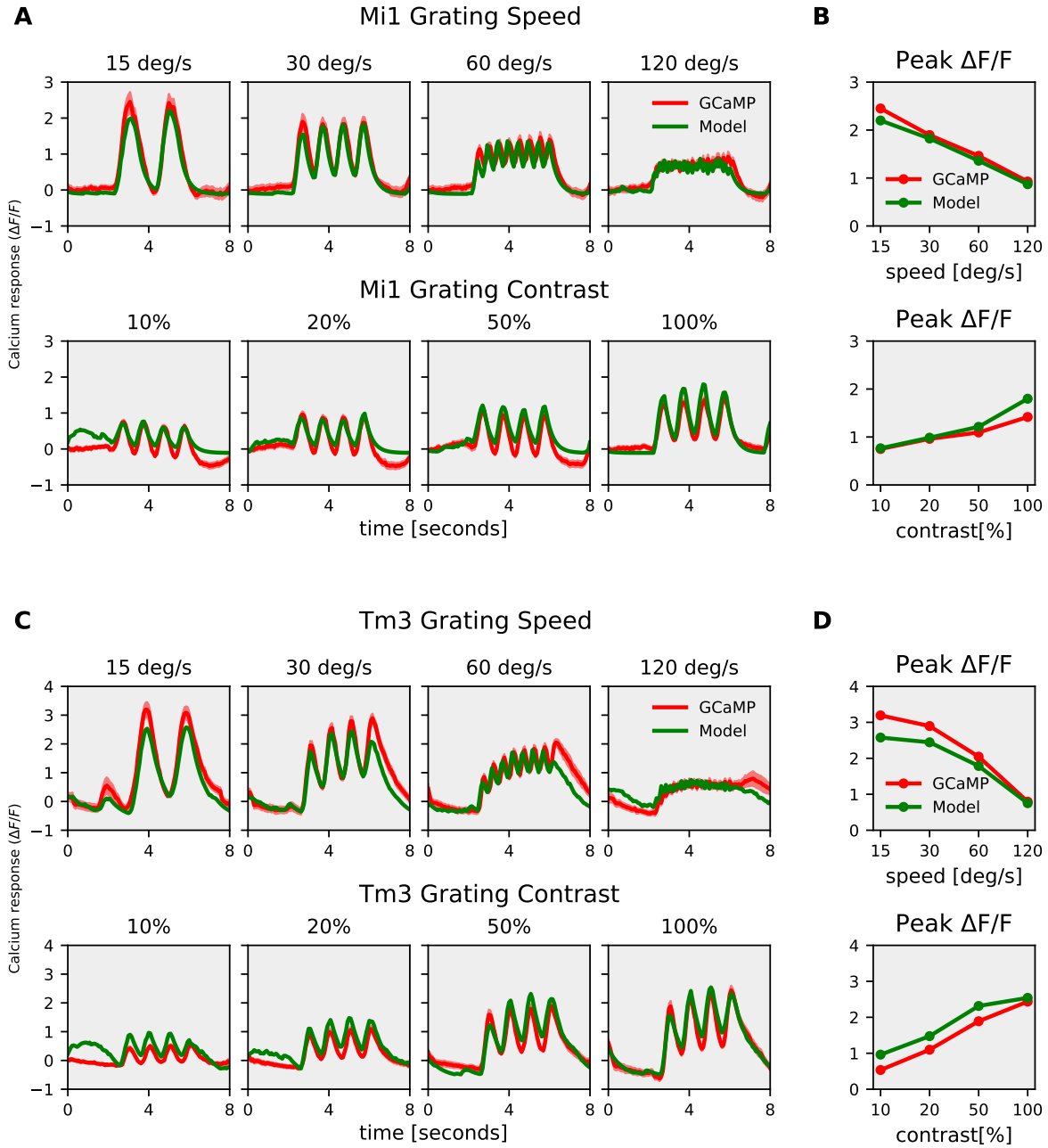


**Figure 8. Mi1, Tm3 Simple model responses** : (A) Mi1 GCaMP (red) & model (green) responses to gratings moving at 4 different speeds (top row) and to gratings moving at 4 different contrasts (bottom row). (B) Mi1 GCaMP & model peak responses to gratings moving at 4 different speeds (top) and 4 different contrasts (bottom). (C) Tm3 GCaMP (red) & model (green) responses to gratings moving at 4 different speeds (top row) and to gratings moving at 4 different contrasts (bottom row). (D) Tm3 GCaMP & model peak responses to gratings moving at 4 different speeds (top) and 4 different contrasts (bottom).

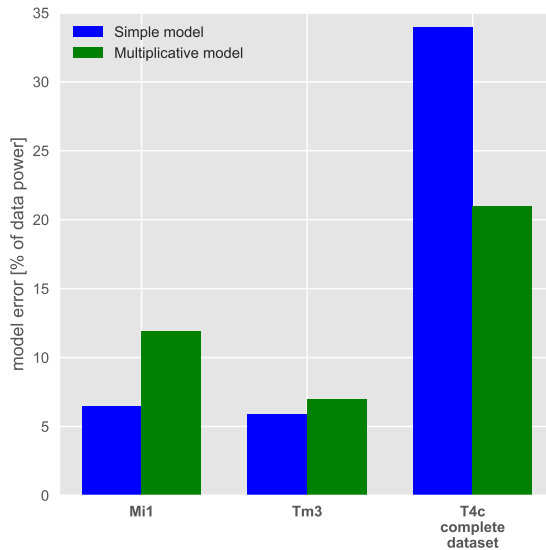


**Figure 9. Model error for the Simple and Multiplicative model :** The model error calculated as  $(\text{Model data} - \text{Experiment data})^2 / (\text{Experiment data})^2$  for the Simple model (blue) and Multiplicative model (green). Mi1 and Tm3 dataset consists of gratings at 4 different speeds and contrast moving in a single direction. T4c complete dataset consists of gratings moving in 12 different directions, and ON edge moving in PD, ND at 4 different speeds and contrasts i.e. a total of 112 stimuli conditions.

To allow only GCaMP emission spectrum to be detected, a band-pass filter (Brightline 520/35) was placed in-front of the photomultiplier. For all stimuli used here, we set the medium brightness to a 8-bit grayscale value of 50, which corresponds to a medium luminance of  $55 \pm 11 \text{ cd/m}^2$ . Stimuli were rendered using custom written software in Python 2.7.

### Stimuli

Stimuli were presented with 3-5 repetitions per experiment in a randomized fashion. To measure the directional and speed tuning, square-wave gratings with a spatial wavelength of  $30^\circ$  spanning the full extent of the stimulus arena were used. The gratings were moved in 12 different directions from  $0^\circ - 360^\circ$  at 4 different speed ( $15^\circ \text{ s}^{-1}$ ,  $30^\circ \text{ s}^{-1}$ ,  $60^\circ \text{ s}^{-1}$ ,  $120^\circ \text{ s}^{-1}$ ). Similarly, to measure direction and contrast tuning, square-wave gratings with a spatial wavelength of  $30^\circ$  spanning the full extent of the stimulus arena were used. The gratings moved at a speed of  $30^\circ \text{ s}^{-1}$  in 12 different directions at 4 different contrast (10%, 20%, 50%, 100%). Edge responses were measured using ON edge i.e. bright edge moving on a dark background with full contrast. The ON edge moved in preferred direction (upward) or null direction (downward) at 4 different speed ( $15^\circ \text{ s}^{-1} - 120^\circ \text{ s}^{-1}$ ).

### Data analysis

Data analysis was performed using custom-written routines in Matlab and Python 2.7, 3.7. Images were automatically registered using horizontal and vertical translations to correct for the movement of brain. Fluorescence changes ( $\Delta F/F$ ) were then calculated using a standard baseline algorithm (Jia *et al.* 2011). Regions of interest (ROIs) were drawn on the average raw image manually by hand in the medulla layer M10 for signals from T4 dendrites. Averaging the fluorescence change over this ROI in space resulted in a ( $\Delta F/F$ ) time course. Voltage imaging with ArcLight and Calcium imaging with GCaMP were performed and analysed using same settings.



## References

1. Denk, W., Strickler, J. H. & Webb, W. W. Two-photon laser scanning fluorescence microscopy. *Science* **248**, 73–76 (1990). doi: [10.1126/science.2321027](https://doi.org/10.1126/science.2321027)
2. Littleton, J. T. & Ganetzky, B. Ion channels and synaptic organization: analysis of the *Drosophila* genome. *Neuron* **26**, 35–43 (2000). doi: [10.1016/s0896-6273\(00\)81135-6](https://doi.org/10.1016/s0896-6273(00)81135-6)
3. Chapman, E. R. Synaptotagmin: a Ca<sup>2+</sup> sensor that triggers exocytosis? *Nature Reviews Molecular Cell Biology* **3**, 498–508 (2002). doi: [10.1038/nrm855](https://doi.org/10.1038/nrm855)
4. Polgruto, T. A., Sabatini, B. L. & Svoboda, K. ScanImage: flexible software for operating laser scanning microscopes. *Biomedical engineering online* **2**, 1–9 (2003). doi: [10.1186/1475-925X-2-13](https://doi.org/10.1186/1475-925X-2-13)
5. Murata, Y., Iwasaki, H., Sasaki, M., Inaba, K. & Okamura, Y. Phosphoinositide phosphatase activity coupled to an intrinsic voltage sensor. *Nature* **435**, 1239–1243 (2005). doi: [10.1038/nature03650](https://doi.org/10.1038/nature03650)
6. King, G. F. Modulation of insect CaV channels by peptidic spider toxins. *Toxicon* **49**, 513–530 (2007). doi: [10.1016/j.toxicon.2006.11.012](https://doi.org/10.1016/j.toxicon.2006.11.012)
7. Di Maio, V. Regulation of information passing by synaptic transmission: a short review. *Brain research* **1225**, 26–38 (2008). doi: [10.1016/j.brainres.2008.06.016](https://doi.org/10.1016/j.brainres.2008.06.016)
8. Gu, H. *et al.* Cav2-type calcium channels encoded by cac regulate AP-independent neurotransmitter release at cholinergic synapses in adult *Drosophila* brain. *Journal of neurophysiology* **101**, 42–53 (2009). doi: [0.1152/jn.91103.2008](https://doi.org/10.1152/jn.91103.2008)
9. Joesch, M., Schnell, B., Raghu, S. V., Reiff, D. F. & Borst, A. ON and OFF pathways in *Drosophila* motion vision. *Nature* **468**, 300–304 (2010). doi: [10.1038/nature09545](https://doi.org/10.1038/nature09545)
10. Eichner, H., Joesch, M., Schnell, B., Reiff, D. F. & Borst, A. Internal structure of the fly elementary motion detector. *Neuron* **70**, 1155–1164 (2011). doi: [10.1016/j.neuron.2011.03.028](https://doi.org/10.1016/j.neuron.2011.03.028)
11. Jia, H., Rochefort, N. L., Chen, X. & Konnerth, A. In vivo two-photon imaging of sensory-evoked dendritic calcium signals in cortical neurons. *Nature protocols* **6**, 28–35 (2011). doi: [10.1038/nprot.2010.169](https://doi.org/10.1038/nprot.2010.169)
12. Jin, L. *et al.* Single action potentials and subthreshold electrical events imaged in neurons with a fluorescent protein voltage probe. *Neuron* **75**, 779–785 (2012). doi: [10.1016/j.neuron.2012.06.040](https://doi.org/10.1016/j.neuron.2012.06.040)
13. Cao, G. *et al.* Genetically targeted optical electrophysiology in intact neural circuits. *Cell* **154**, 904–913 (2013). doi: [10.1016/j.cell.2013.07.027](https://doi.org/10.1016/j.cell.2013.07.027)
14. Chen, T.-W. *et al.* Ultrasensitive fluorescent proteins for imaging neuronal activity. *Nature* **499**, 295–300 (2013). doi: [10.1038/nature12354](https://doi.org/10.1038/nature12354)
15. Iniguez, J., Schutte, S. S. & O'Dowd, D. K. Cav3-type  $\alpha 1T$  calcium channels mediate transient calcium currents that regulate repetitive firing in *Drosophila* antennal lobe PNs. *Journal of neurophysiology* **110**, 1490–1496 (2013). doi: [10.1152/jn.00368.2013](https://doi.org/10.1152/jn.00368.2013)
16. Maisak, M. S. *et al.* A directional tuning map of *Drosophila* elementary motion detectors. *Nature* **500**, 212–216 (2013). doi: [10.1038/nature12320](https://doi.org/10.1038/nature12320)
17. Mazurek, M., Kager, M. & Van Hooser, S. D. Robust quantification of orientation selectivity and direction selectivity. *Frontiers in neural circuits* **8**, 92 (2014). doi: [10.3389/fncir.2014.00092](https://doi.org/10.3389/fncir.2014.00092)
18. Arenz, A., Drews, M. S., Richter, F. G., Ammer, G. & Borst, A. The temporal tuning of the *Drosophila* motion detectors is determined by the dynamics of their input elements. *Current Biology* **27**, 929–944 (2017). doi: [10.1016/j.cub.2017.01.051](https://doi.org/10.1016/j.cub.2017.01.051)
19. Takemura, S.-y. *et al.* The comprehensive connectome of a neural substrate for 'ON'motion detection in *Drosophila*. *Elife* **6**, e24394 (2017). doi: [10.7554/eLife.24394](https://doi.org/10.7554/eLife.24394)

- 333 20. Borst, A., Haag, J. & Mauss, A. S. How fly neurons compute the direction of visual motion.  
334 *Journal of Comparative Physiology A* **206**, 109–124 (2020). doi: [10.1007/s00359-019-01375-9](https://doi.org/10.1007/s00359-019-01375-9)
- 335 21. Davis, F. P. *et al.* A genetic, genomic, and computational resource for exploring neural circuit  
336 function. *Elife* **9**, e50901 (2020). doi: [10.7554/eLife.50901](https://doi.org/10.7554/eLife.50901)
- 337 22. Luo, L. *Principles of neurobiology* (Garland Science, 2020). doi: [10.1201/9781003053972](https://doi.org/10.1201/9781003053972)
- 338 23. Virtanen, P. *et al.* SciPy 1.0: fundamental algorithms for scientific computing in Python. *Nature*  
339 *methods* **17**, 261–272 (2020). doi: [10.1038/s41592-019-0686-2](https://doi.org/10.1038/s41592-019-0686-2)
- 340 24. Zhang, Y. *et al.* jRCaMP1a Fast genetically encoded calcium indicators. *Online resource* (2020).  
341 doi: [10.25378/janelia.13148243.v4](https://doi.org/10.25378/janelia.13148243.v4)
- 342 25. Groschner, L. N., Malis, J. G., Zuidinga, B. & Borst, A. A biophysical account of multiplication by  
343 a single neuron. *Nature* **603**, 119–123 (2022). doi: [10.1038/s41586-022-04428-3](https://doi.org/10.1038/s41586-022-04428-3)